Archival Report

Biological Psychiatry

Transcriptional Profiling of Primate Central Nucleus of the Amygdala Neurons to Understand the Molecular Underpinnings of Early-Life Anxious Temperament

Rothem Kovner, Tade Souaiaia, Andrew S. Fox, Delores A. French, Cooper E. Goss, Patrick H. Roseboom, Jonathan A. Oler, Marissa K. Riedel, Eva M. Fekete, Julie L. Fudge, James A. Knowles, and Ned H. Kalin

ABSTRACT

BACKGROUND: Children exhibiting extreme anxious temperament (AT) are at an increased risk for developing anxiety and depression. Our previous mechanistic and neuroimaging work in young rhesus monkeys linked the central nucleus of the amygdala to AT and its underlying neural circuit.

METHODS: Here, we used laser capture microscopy and RNA sequencing in 47 young rhesus monkeys to investigate AT's molecular underpinnings by focusing on neurons from the lateral division of the central nucleus of the amygdala (CeL). RNA sequencing identified numerous AT-related CeL transcripts, and we used immunofluorescence ($n = 3$) and tract-tracing ($n = 2$) methods in a different sample of monkeys to examine the expression, distribution, and projection pattern of neurons expressing one of these transcripts.

RESULTS: We found 555 AT-related transcripts, 14 of which were confirmed with high statistical confidence (false discovery rate $< .10$), including protein kinase C delta (PKCδ), a CeL microcircuit cell marker implicated in rodent threat processing. We characterized PKCδ neurons in the rhesus CeL, compared its distribution with that of the mouse, and demonstrated that a subset of these neurons project to the laterodorsal bed nucleus of the stria terminalis.

CONCLUSIONS: These findings demonstrate that CeL PKCδ is associated with primate anxiety, provides evidence of a CeL to laterodorsal bed nucleus of the stria terminalis circuit that may be relevant to understanding human anxiety, and points to specific molecules within this circuit that could serve as potential treatment targets for anxiety disorders.

Keywords: Anxiety, Bed nucleus of the stria terminalis, Central nucleus of the amygdala, Fear, Microcircuitry, Protein kinase C delta (PKCδ), Retrograde tracing, Somatostatin, Stress

https://doi.org/10.1016/j.biopsych.2020.05.009

Depending on its intensity and context in which it is expressed, anxiety can be adaptive or maladaptive. Across a population, anxiety is characterized by individual differences and when extreme is disabling. Research has identified heritable and nonheritable factors underlying the development of anxiety disorders (1–4), and during childhood these can manifest as the trait-like disposition anxious temperament (AT). Like anxiety, AT is dimensional and is characterized by individual differences in inhibitory responses to novel and social situations (5–8) as well as threat-related pituitary–adrenal activation (5,9). Because AT reflects a combination of behavioral and physiological responses to stress, this construct reflects the interplay among emotions, behavior, and physiology that is emblematic of anxiety responses. When extreme and stable over time, childhood AT increases the risk for the development of anxiety disorders, depression, and comorbid substance use disorder later in life (6,7,10–12).

To understand the mechanisms underlying AT, we developed a young rhesus monkey model of individual differences in the expression of dispositional anxiety that is analogous to the phenotype exhibited by at-risk children (13,14). Rhesus monkeys are ideally suited for studies of human psychopathology owing to their recent evolutionary divergence from humans, which is reflected in similarities in brain structure and in their emotional and physiological responding (14). Our approach is to understand individual differences in the AT phenotype in relation to individual differences in its underlying neural and molecular substrates (4,13,15). Using a large multigenerational pedigree, we demonstrated that AT is ~30% heritable, consistent with previous human studies (4,16).

ISSN: 0006-3223

Numerous studies point to the importance of the extended amygdala in mediating adaptive responses to threat as well as in stress-related psychopathology (13,17,18). Components of the extended amygdala include the central nucleus of the amygdala (Ce) and the bed nucleus of the stria terminalis (BST) (19). The Ce, primarily composed of GABAergic (gamma-aminobutyric acidergic) neurons, coordinates information flow out of the amygdala (20–24). The Ce sends strong projections to the BST, a region also involved in threat responding (25–27). We previously demonstrated that individual differences in Ce and BST metabolism relate to trait-like individual differences in AT (5), that brain metabolism in these regions is heritable, and that BST metabolism, but not Ce metabolism, is coheritable with AT (4). We also demonstrated that neurotoxic lesions of the Ce reduce AT, directly implicating the Ce as a core mechanistic component of the AT circuit (4,28,29).

It is important to emphasize that the Ce is not uniform and can be divided into at least 2 subnuclei, namely the lateral Ce (CeL) and medial Ce (CeM) (30,31). The CeM coordinates the output of the amygdala via its projections to multiple downstream effector sites (24). The CeL modulates the CeM, helping to orchestrate the different behavioral and physiological responses mediated by the CeM's targets (21,32). The entire Ce projects to the BST to further coordinate threat-related responding, where the CeL's projections are largely restricted to the laterodorsal BST (BSTLd) (25,33–35). In addition to other basal forebrain areas, the CeL, CeM, and BSTLd have been conceptualized as the central extended amygdala (19). Rodent studies have traced microcircuits within the extended amygdala that are composed of GABAergic neuronal subtypes acting to mediate anxiety and fear responses (23,32–35). However, these microcircuits have not yet been characterized in primates.

In this study, we characterized individual differences in gene expression in laser microdissected primate CeL neurons in relation to AT and its components by performing RNA sequencing (RNA-Seq). We focused on CeL neurons because of their mechanistic role in mediating primate AT and because of rodent data demonstrating the CeL's role in integrating information and acting as an interface between the basolateral amygdala and the CeM/BSTLd (23,26,36,37). Rodent studies have also highlighted subpopulations of GABAergic CeL neurons, such as those expressing protein kinase C delta (gene: *Prkcd, PRKCD*; protein: PKCδ) or somatostatin (gene: *Sst, SST*; protein: SST), that have critical roles in modulating fear- and anxiety-related extended amygdala function (20,32,38,39). Here, in addition to our discovery-based approach, we more specifically focused on genes known to distinguish CeL neuronal subtypes. Because the RNA-Seq data revealed relations between *PRKCD* expression and AT, as an initial step to understanding extended amygdala microcircuitry in the primate, we characterized the distribution and projection pattern of PKCδ neurons within the extended amygdala. This approach informs the translational value of rodent anxiety models to primates, and because of the relevance of the rhesus AT model to humans, the findings have the potential to uncover novel molecular targets for the treatment of anxiety disorders and other stress-related psychopathology.

METHODS AND MATERIALS

Complete methods are provided in Supplement 1.

AT Phenotyping

AT is a composite score reflecting threat-related behavioral and cortisol changes elicited by exposure to the no-eye-contact condition of the human intruder paradigm (5). Freezing duration and coo vocalization reductions, along with plasma cortisol levels, were used to compute each individual's AT (Supplement 1).

Animals

A total of 47 monkeys (*Macaca mulatta*; average age = 2.27 years, SD = 0.46; 24 male and 23 female) were used for RNA-Seq. To understand the AT levels in these 47 animals in relation to a larger population from which they came, we performed an analysis with data from animals that were phenotyped in our laboratory over the last 12 years (n = 721, average age = 1.9 years, SD = 0.74; 386 male and 335 female) (Figure S1B in Supplement 1). C57BL/6J and KO;B6;129X1-*Prkcd*^{tm1Msg}/J mice (Jackson Laboratory, Bar Harbor, ME) were group housed for at least 7 days before experimentation (12-hour light/dark cycle; ad libitum access to food and water). When 21 days old, mice were perfused (40) and tissue was stored for immunohistochemical studies. Animal housing and experimental procedures were conducted in accordance with institutional guidelines and were approved by the Committee on the Ethics of Animal Research of the University of Wisconsin–Madison.

Laser Capture Microdissection

All monkeys were euthanized under deep anesthesia, 4 days after AT phenotyping, with the guidance of veterinary staff using pentobarbital, consistent with the recommendations of the Panel on Euthanasia of the American Veterinary Medical Association. Fresh frozen tissue was collected, cut into slabs, flash frozen in 2-methylbutane, and stored at −80°C as previously described (41). Then, 14-μm sections from the slab containing the amygdala were obtained on a cryostat at −20°C. Sections throughout the CeL's anterior–posterior (A-P) extent were mounted on Leica PEN (polyethylene napthalate) 2.0-μm membrane laser capture microdissection (LCM) slides (11532918; Leica, Wetzlar, Germany). Adjacent sections were stained with acetylcholinesterase to localize the Ce (Figure S2B in Supplement 1). LCM sections were rapidly stained for NeuN (neuronal nuclei) (Supplement 1). CeL neurons were dissected with a Leica LMD6500 laser capture microscope. For each animal, 500 to 600 neurons were sampled from 6 to 8 slides (every 0.25 mm). After dissection, each LCM slide image was overlaid with its adjacent acetylcholinesterase slide image in Adobe Illustrator CC 2014 to confirm that cells were dissected from the CeL. Tubes containing a minimum of 80% of neurons captured from the CeL were used, and the percentage of CeL neurons in each of these tubes was used to calculate a CeL neuronal accuracy score (Supplement 1). Within an animal, tubes were pooled for RNA extraction using Qiagen RNeasy Plus Micro kit (74034; Qiagen, Hilden, Germany).

RNA Sequencing

RNA was sequenced at the University of Southern California by JAK. Samples were processed with NuGen RNA-Seq V2 kit

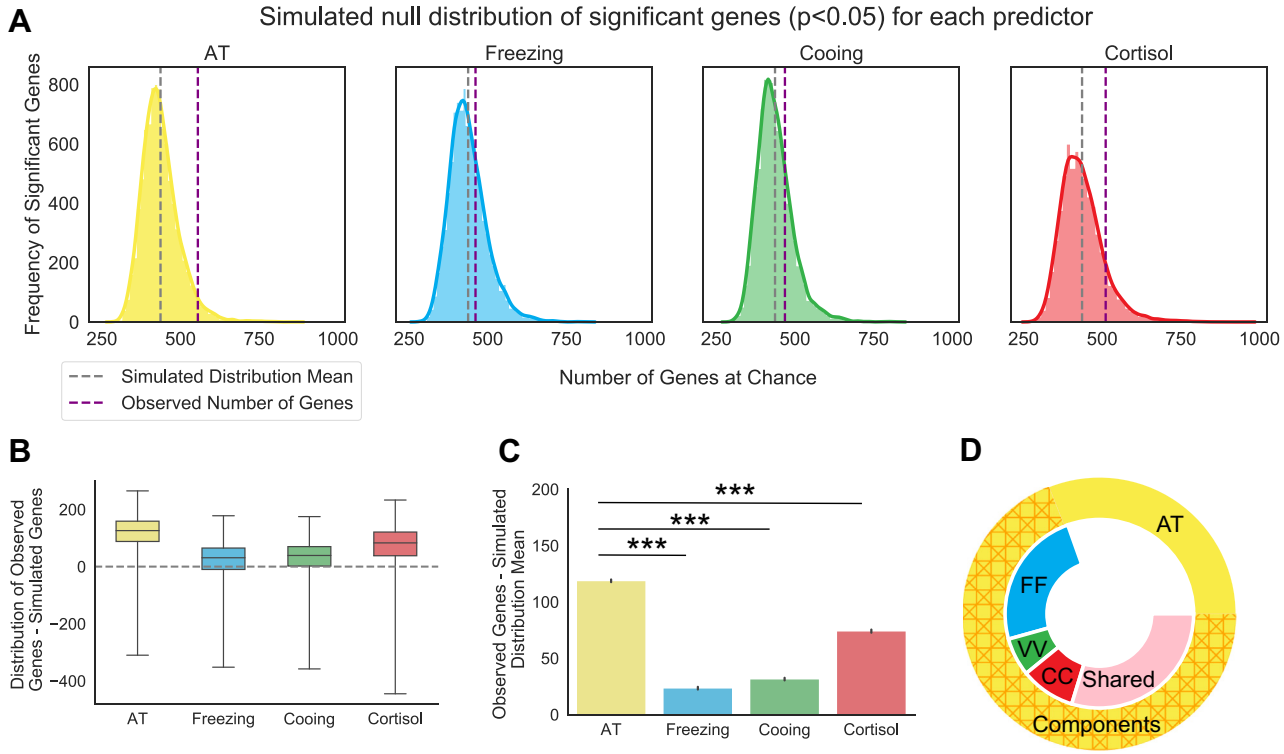

Figure 1. AT predicts a significant number of genes above chance and outperforms each of the AT components. **(A)** Simulated null distribution (as described in Methods and Materials) for each predictor of interest at a nominal p value of $p < .05$. Purple dotted lines indicate the observed number of genes associated with each predictor's real values. Gray dotted lines indicate the mean number of genes of the simulated distribution. The solid colored outline of the distribution represents the density of significant genes as determined by a kernel density estimation. **(B)** Boxplots for each predictor depicting the distribution and mean of the differences between the real observation and each simulated value. Empirical p values were calculated for each predictor (AT: $p = .04$; freezing: $p = .30$; cooing: $p = .24$; cortisol: $p = .12$). **(C)** Barplot demonstrating that AT predicts significantly more genes above the simulated distribution mean than those predicted by each of the AT components alone: freezing ($t = 113.5$, $p < .001$), cooing ($t = 106.9$, $p < .001$), or cortisol ($t = 496$, $p < .001$). Error bars are displayed as SEM. The p values are Šidák corrected for multiple comparisons. AT component values were transformed and residualized as described in Methods and Materials. **(D)** Donut plot depicting the number of overlapping genes between individual AT components and AT. Outside circle represents all 555 AT-related genes ($p < .05$) and is separated into the 383 genes that overlap with AT components (hashed orange) and the 172 genes that are unique to AT (yellow). Inner circle represents genes that are related to AT and is broken up by genes that are also unique to one AT component (FF: freezing in blue; VV: cooing in green; CC: cortisol in red) or that are shared by at least 2 components (shared in pink). ***significant at $p < .0001$. AT, anxious temperament.

(7102-32; NuGen, San Carlos, CA) for complementary DNA synthesis and with NuGEN Ovation Rapid Library kit (0319 and 0320) for library preparation. The Illumina HiSeq 2500 with regular rapid sequencing prep kit was used (Illumina, San Diego, CA). Reads were single end and targeted to be 100 base pairs in length. A mean of 949710 mapped reads was found across animals. Reads were mapped to MacaM 7.8 (42). Mapping was performed using Sequence Alignment for Gene Expression (https://github.com/tadesouaiaia/sage) written in Python 2.7.

RNA-Seq Analysis and Model Evaluation

Genes with 1 read in at least 20% of the animals were used for quantile normalization. Data were log2 transformed, and fully annotated genes where at least 50% of the samples expressed more than 1 mapped read were used in ordinary least squares (OLS) regression. We built statistical models that assessed the association between gene expression and the predictor of interest. AT, freezing, cooing, and cortisol measured closest to time of death were used as predictors. The statistical model was built within a framework designed to maximize power to detect predictor-related associations while also reducing false positives discovered with permutation analysis. We focused on models that described the largest fraction of the variance (R^2) across the transcriptome without overfitting.

Variables were tested in relation to transcriptome-wide gene expression to identify potential covariates and were tested for collinearity (Figure S3A in Supplement 1). Two measures (CeL neuron accuracy and age at necropsy) were selected because they were not multicollinear and had the greatest number of positive genes relative to false positives in a simulation (Supplement 1 and Table S1 in Supplement 2). Using CeL neuron accuracy and age at necropsy as covariates separately and together, we tested models to establish whether they could detect predictor-related gene expression relationships above chance. Sex was not included because it did not perform better than a pseudovariable and did not improve upon the variance accounted for by a model without sex (Table S2 in Supplement 2). We chose the models using both neuron accuracy and age at necropsy because they had the

Table 1. Verified Gene Hits That Pass Multiple Comparison Correction Across Two Different Statistical Methods

Gene	Functions of Interest[a]	AT Relation[b]
chr18: *SS18*	Nuclear receptor transcription coactivator activity (GO:0030374) Positive regulation of transcription, DNA templated (GO:0045893)	–
chr02a: *DNMT3A*	DNA binding (GO:0003677) Chromatin binding (GO:0003682)	+
chr05: *ZNF300*	Sequence-specific DNA binding (GO:0043565)	–
chr03: *PRKCD*	Intracellular signal transduction (GO:0035556) Protein kinase C activity (GO:0004697)	+
chr06: *SH3BGRL2*	SH3 domain binding (GO:0017124)	+
chr15: *BCR*	Protein binding (GO:0005515)	+
chr16: *FBXL16*	Ubiquitin–protein transferase activity (GO:0004842)	+
chr02a: *AFTPH*	Clathrin binding (GO:0030276) Intracellular transport (GO:0046907)	+
chr17: *DYNLL2*	Dynein light intermediate chain binding (GO:0051959)	–
chr10: *SLC18A2*	Monoamine transmembrane transporter activity (GO:0008504)	+
chr06: *KIAA1009*	Protein binding (GO:0005515)	–
chr01: *MGST3*	Glutathione transferase activity (GO:0004364)	+
chr09: *KIAA1045*	Regulation of synaptic transmission, GABAergic (GO:0032228)	+
chr16: *C16orf87*	Protein binding (GO:0005515)	+

AT, anxious temperament; GABAergic, gamma-aminobutyric acidergic; GO, Gene Ontology.
[a]Functions of interest were chosen based on ontologies that contain these genes.
[b]AT relation indicates the direction of the gene expression correlation with AT.

lowest Bayesian information criterion, accounted for the greatest percentage of the variance, and had the fewest false positives in a simulated model. In the models using AT, freezing, cooing, and cortisol as predictors, the predictor was shuffled and correlated with gene expression. Chance distributions were constructed with 10,000 simulations for each predictor (Figure 1A) to assess the signal strength relative to noise. The final model was used to determine differentially expressed genes associated with each predictor. OLS regression and permutation testing (Supplement 1) were performed in Python 2.7. Another differential gene expression analysis was performed using DESeq2 (43). Gene ontologies were investigated using Panther (44).

RESULTS

AT as a Predictor of the CeL Neuronal Transcriptome Compared With Its Individual Components

LCM was combined with RNA-Seq to identify CeL neuronal gene expression (Figures S2A and S3B, C in Supplement 1) associated with individual differences in AT and its components (Figure 1A). Because our previous work demonstrated that AT accounts for greater variance in CeL metabolism than its components (45), we explored the hypothesis that AT would better predict gene expression than each of its components. After demonstrating that the AT scores of the 47 animals used here were representative of a larger population (n = 721) (Figure S1B and Supplemental Results in Supplement 1), multiple regression was used to investigate the relation between gene expression and each predictor (AT, freezing, cooing, and cortisol). We performed a permutation analysis where 10,000 shuffles were performed for each predictor and correlated with transcript expression to construct simulated null distributions of the number of genes associated with each predictor at chance (Figure 1A). Results demonstrated that AT performed significantly better than chance (empirical p = .04) (Figure 1B), whereas AT's individual components did not. Furthermore, the number of genes that were above chance predicted by AT was significantly greater than the number predicted by AT's components (Figure 1C). In total, 555 genes were significantly associated with AT, 383 genes were significantly associated with at least one of AT's components, and 172 genes were significantly and selectively correlated with AT (Figure 1D, Supplemental Results, and Figure S5 in Supplement 1). A similar pattern was observed after performing a weighted gene coexpression network analysis (Supplemental Results and Figure S6 in Supplement 1).

Specific CeL Neuronal Transcripts Associated With AT

Two different approaches were used to identify AT-associated genes. Using DESeq2 (43), which uses a negative binomial model, we identified 716 AT-related genes ($p < .05$) (Table S2 in Supplement 2), constituting 11% of the total genes tested, with 42 genes passing multiple comparison correction (false discovery rate [FDR] $< .10$). In addition, we also used an OLS approach with log-transformed data, which identified 555 AT-related transcripts, comprising 6% of the total genes tested ($p < .05$) (Table S2 in Supplement 2). To account for multiple testing, we performed a nonparametric permutation test on the correlation between AT and gene expression, identifying 20 genes (FDR $< .10$) (Supplement 1). The conjunction of the FDR-corrected genes between the DESeq2 and OLS analyses yielded 14 genes (Table 1 and Table S2 in Supplement 2). Gene Ontology (GO) enrichment analyses on the genes identified with each approach (Figure 2A) demonstrated several biological processes (Table S3 in Supplement 2) in common,

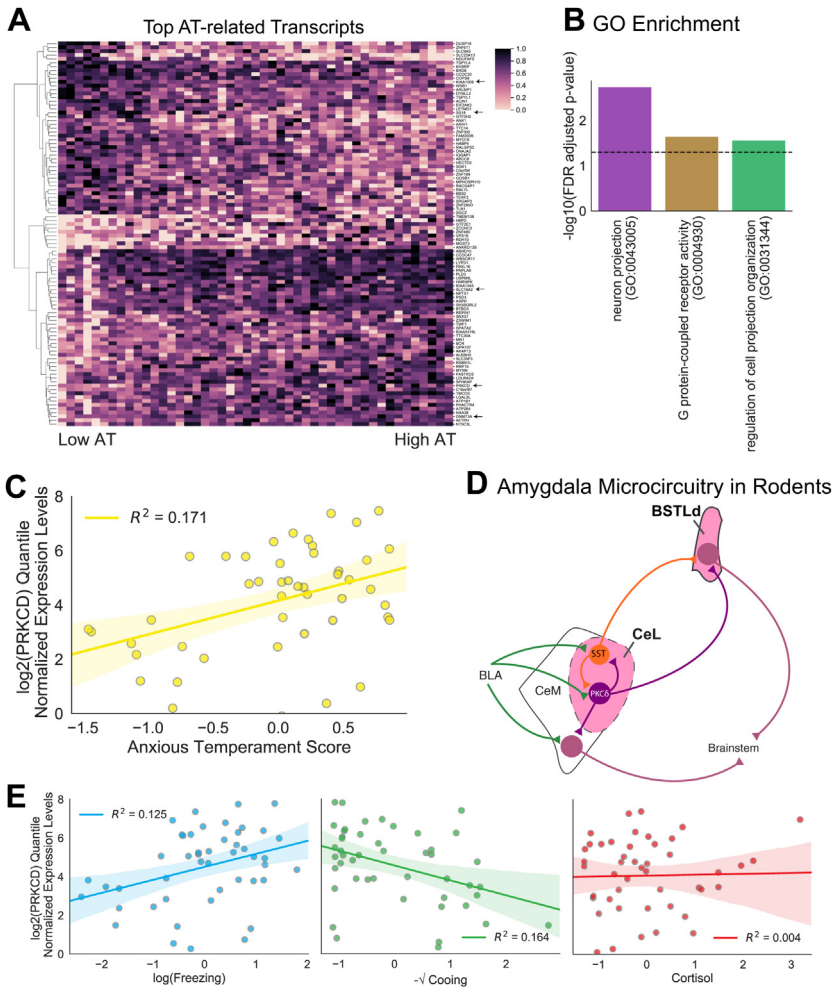

Figure 2. RNA-Seq of LCM CeL neurons revealed AT-related genes. **(A)** Heatmap displaying the top 100 AT-related genes from the intersection of the OLS and DESeq2 analyses ($p < .05$). Gene expression data are presented as quantile normalized min–max scaled values. Arrows point to genes that are discussed in the text. **(B)** Subset of GO enrichment groups for cellular component (purple), molecular function (yellow), and biological process (green) that overlap between approaches. The FDR-corrected p value is depicted by the black dashed line. FDR values reflect those from the OLS ontology. All statistics can be found in Table S2 in Supplement 2. **(C)** Correlation between *PRKCD* mRNA expression levels and AT (R^2 = .171). Shaded areas represent the SEM. **(D)** Simplified diagram of the microcircuit within the rodent amygdala and extended amygdala. PKCδ-expressing neurons are labeled in purple. SST-expressing neurons are labeled in orange. Previous work demonstrated that both SST- and PKCδ-expressing neurons receive information from the BLA and contribute to an inhibitory microcircuit within the CeL (32,38,39). Both cell types also project to the BSTLd, while PKCδ-expressing neurons, but not SST-expressing neurons, project to the CeM (32,38,39). **(E)** Correlations between *PRKCD* mRNA expression levels and the individual components of AT (freezing: R^2 = .125; cooing: R^2 = .164; cortisol: R^2 = .004; OLS regression). Freezing, cooing, and cortisol values were standardized, transformed, and residualized as described in Methods and Materials. *PRKCD* mRNA expression levels are presented as quantile normalized log2 transformed values residualized for age at ToD and CeL neuron accuracy. AT, anxious temperament; BLA, basolateral amygdala complex; BSTLd, laterodorsal bed nucleus of the stria terminalis; CeL, lateral division of the central nucleus of the amygdala; CeM, medial division of the central nucleus of the amygdala; FDR, false discovery rate; GO, Gene Ontology; LCM, laser capture microdissection; mRNA, messenger RNA; PKCδ, protein kinase C delta; OLS, ordinary least squares; RNA-Seq, RNA sequencing; SST, somatostatin; ToD, time of death.

including neuron projection (GO:0043005), cell projection regulation (GO:0031344), and G-protein receptor activity (GO:0031344) (Figure 2B and Table S3 in Supplement 2).

Among the 14 transcripts that passed FDR correction with both methods, several were related to epigenetic mechanisms such as *SS18* (the SS18 subunit of BAF chromatin remodeling complex) and *DNMT3A* (DNA methyltransferase 3). Also of interest was *KIAA1009* because of its role in primary cilia function in adult cells (46) and its link to schizophrenia (47) and cognitive function (48–50). Another potentially exciting transcript was *SLC18A2* (solute carrier family 18 member A2), a vesicular transport protein critical to monoaminergic neurotransmission (51–54). We also identified *PRKCD* (Figure 2A, C), which is particularly interesting because in rodents it marks a CeL neuron population involved in threat processing and Pavlovian learning (Figure 2D) (32,55,56). CeL *PRKCD* neurons decrease their firing in response to a conditioned stimulus and interact with SST neurons to increase freezing behavior (32). In addition, studies demonstrate that CeL *PRKCD* neurons project to the BST (39), and some of these cells play a role in negative reinforcement learning (55). Moreover, neurotrophic signaling, which is associated with AT and neuropsychiatric disorders (41,51,57,58), interacts with PKCδ (52). In addition, *PRKCD* messenger RNA (mRNA) expression was also associated with increased freezing and decreased cooing but not with threat-related cortisol (Figure 2E), suggesting that it may be more strongly associated with the behavioral components of AT.

Characterizing PKCδ and SST Neurons in the Monkey CeL

While PKCδ has been extensively studied in the rodent CeL (32,39,53,55,56), little is known about its expression in the monkey. Within the CeL, many neuronal subtypes exist (54,59–61), and mouse studies reveal that SST neurons modulate PKCδ neurons (22,38,62). Because these cell types have not been well characterized in monkeys, we used stereological cell counting to map CeL PKCδ and SST neurons (Figure 3). To further understand the extent to which the mouse studies are translatable to primates, we also performed studies in the mouse CeL (Figure 3B, C). In the monkey CeL, PKCδ neurons accounted for 59% of the estimated total neurons and

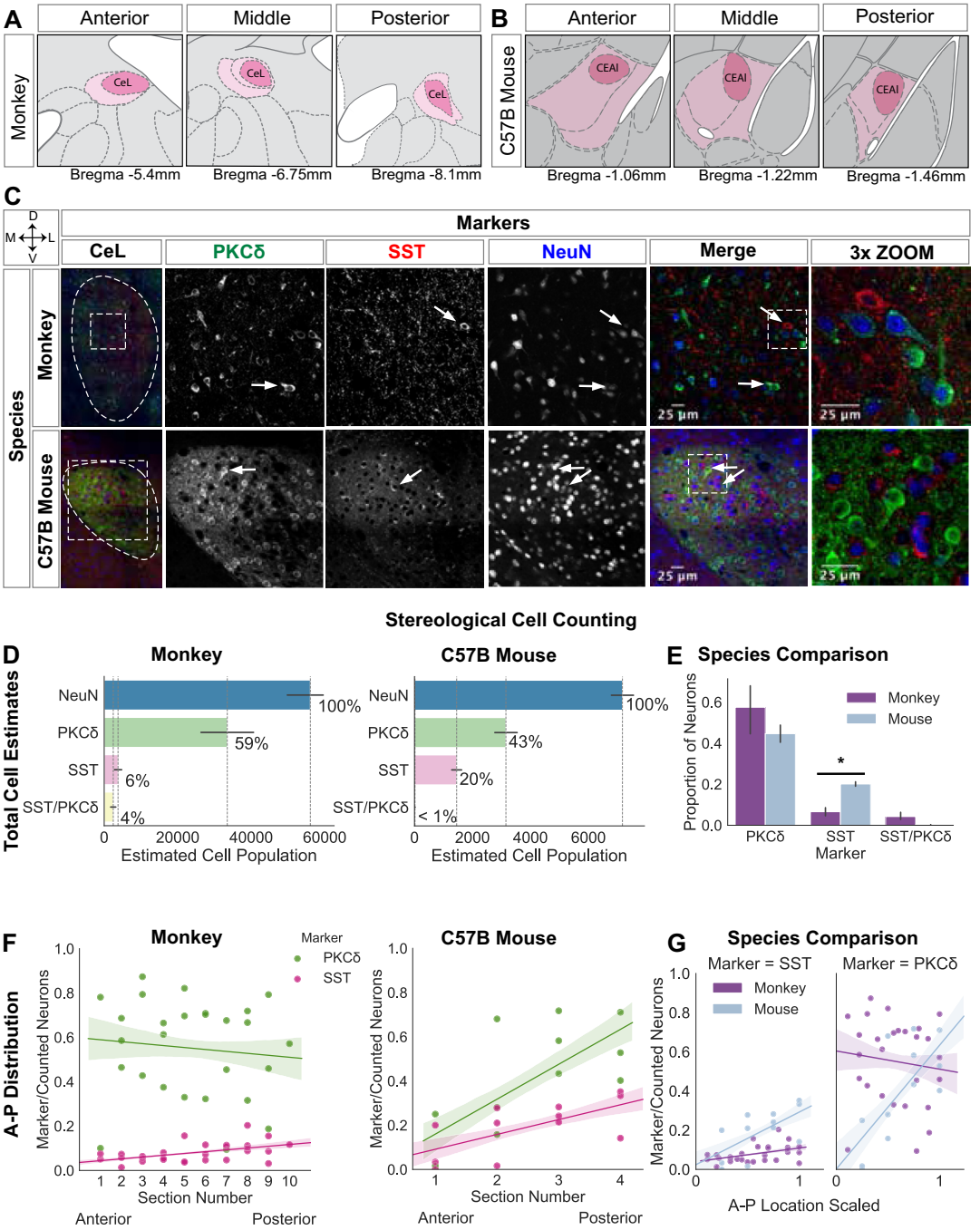

Figure 3. PKCδ- expressing neurons in the monkey CeL compared with the mouse CeL. **(A, B)** CeL atlas slices depicting the A-P extent in the rhesus monkey **(A)** (83) and in the mouse **(B)** (Allen Brain Atlas). **(C)** Representative confocal images of the CeL in both species. White arrows point to PKCδ and SST neurons. Images were adjusted using the Fiji despeckle filter (84) for removing salt and pepper noise. **(D)** Stereological cell estimates for monkey (n = 3) and mouse (n = 3). **(E)** Species comparison of PKCδ, SST, and PKCδ/SST estimates are presented as a proportion of the total number of neurons (PKCδ: $t = -1.06$, $p = .34$; SST: $t = 3.6$, $p = .02$; t test). Error bars are SEM. **(F)** A-P distribution of PKCδ- and SST-expressing neurons in monkey and mouse (monkey: PKCδ $t = -0.39$, $p = .70$ and SST $t = 2.7$, $p = .012$; mouse: PKCδ $t = 3.1$, $p = .01$ and SST $t = 2.6$, $p = .02$; OLS regression). **(G)** Species comparison of the A-P distribution of each cell type: A-P location × species interaction for PKCδ ($t = 2.6$, $p = .01$) and A-P location × species interaction for SST ($t = 2.7$, $p = .01$); OLS regression. To compare A-P distribution between species, A-P location was min–max scaled, with 0 indicating more anterior slices and 1 indicating more posterior slices. A-P, anterior–posterior; CeL, lateral division of the central nucleus of the amygdala; NeuN, neuronal nuclei; OLS, ordinary least squares; PKCδ, protein kinase C delta; SST, somatostatin.

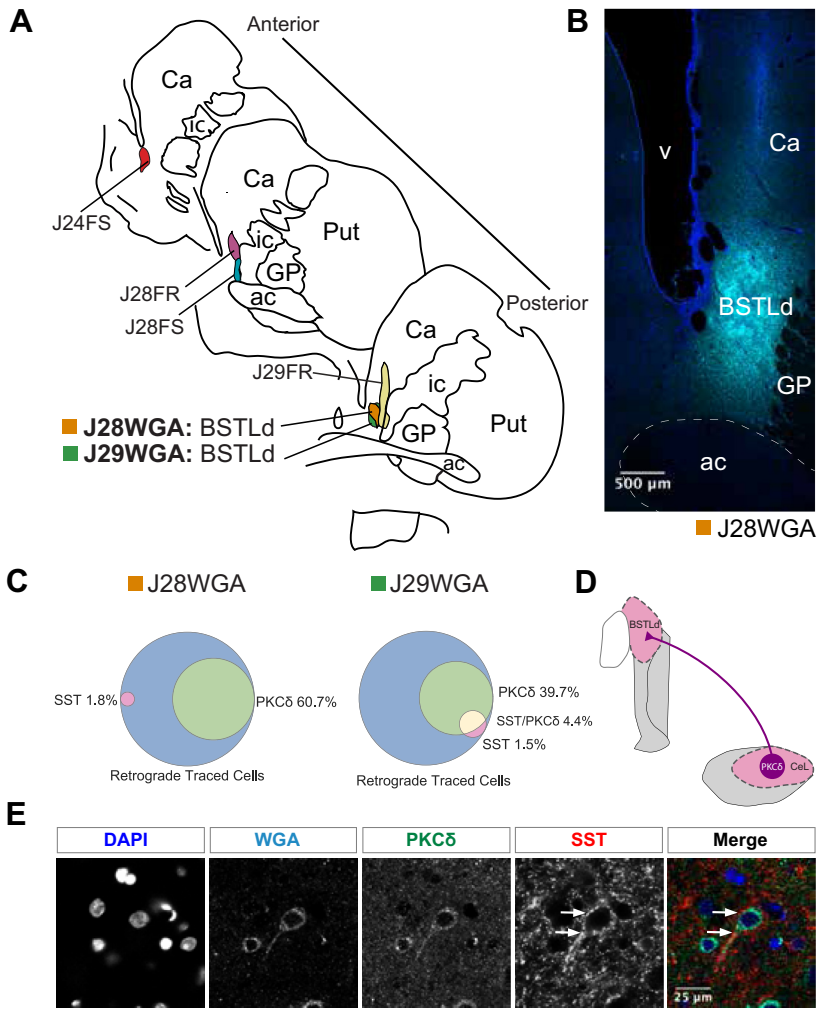

Figure 4. A subset of PKCδ-expressing neurons project to the BSTLd in the monkey. **(A)** Hand-drawn slices depicting the localization of retrograde tracer into different regions of the BST in monkey. Two replicates, J29WGA and J28WGA, are localized to the same part of the BSTLd. **(B)** Representative confocal image of the BSTLd injection site. DAPI staining is in blue. WGA tracer staining is in cyan. **(C)** A Venn diagram for each BSTLd replicate, J29WGA and J28WGA, illustrating the percentage overlap between the WGA tracer and PKCδ, SST, or both. **(D)** Simplified diagram of our results demonstrating that CeL PKCδ-expressing neurons project to the BSTLd in nonhuman primates. **(E)** Representative confocal image of a BSTLd-projecting neuron that expresses PKCδ. This image was adjusted using the Fiji despeckle filter (84) for removing salt and pepper noise. White arrows point to the immense SST innervation received along this neuron's primary dendrite and soma. ac, anterior commissure; BST, bed nucleus of the stria terminalis; BSTLd, laterodorsal bed nucleus of the stria terminalis; Ca, caudate; CeL, lateral division of the central nucleus of the amygdala; GP, globus pallidus; ic, internal capsule; PKCδ, protein kinase C delta; Put, putamen; SST, somatostatin; v, ventricle; WGA, wheat germ agglutinin.

SST neurons accounted for 6% (Figure 3D). In the mouse CeL, PKCδ neurons constituted 43% of the estimated total neurons and SST neurons accounted for 20% (Figure 3D). While the proportions of PKCδ neurons did not significantly differ between species ($t = -1.06$, $p = .34$) (Figure 3E), the proportion of SST cells was notably decreased in the monkey compared with the mouse ($t = -3.6$, $p = .02$) (Figure 3E). In monkeys 4% of neurons expressed SST and PKCδ, while in mice this population was nonexistent (Figure 3D).

Previous studies demonstrated that cell types are differentially distributed across the Ce's A-P extent, suggesting A-P functional differences (32,63,64). Consistent with this, PKCδ neurons ($t = 3.1$, $p = .01$) and SST neurons ($t = 2.6$, $p = .02$) were significantly more concentrated in the posterior mouse CeL (Figure 3F). In the monkey, SST somata were more concentrated in the posterior CeL ($t = 2.7$, $p = .012$) (Figure 3F), replicating previous observations (65). However, deviating from the mouse, monkey PKCδ neurons were not differentially distributed across the A-P extent ($t = -0.39$, $p = .70$). The interaction between A-P location and species was tested separately for PKCδ and SST neurons and demonstrated significant interactions (PKCδ: $t = 2.6$, $p = .01$; SST: $t = 2.7$, $p = .01$) (Figure 3G).

In contrast to the small number of CeL SST neurons, and consistent with previous work, we found dense SST neuropil throughout the monkey CeL (64–67). Numerous SST varicosities were present in close apposition to the primary dendrite and soma of large CeL neurons, a number of which expressed PKCδ (Figure 3C), suggesting that in monkeys SST input may modulate CeL PKCδ neurons. Compared with the limited distribution profile described in the mouse (32), monkey *PRKCD* expression was widely distributed across the brain (Figure S7 in Supplement 1).

A Subset of CeL PKCδ Neurons Project to the BSTLd in the Monkey

In rodents, in addition to constituting an intra-CeL microcircuit, *Prkcd* and *Sst* neurons project to other parts of the extended

Table 2. Number and Percentage of Retrograde Tracer–Labeled Cells Expressing Markers of Interest for Each Case of Retrograde Injection

Case ID	Retrograde Tracer Type	Number of Retrograde-Labeled Cells	Retrograde-Labeled Cells Expressing PKCδ		Retrograde-Labeled Cells Expressing SST		Retrograde-Labeled Cells Expressing PKCδ and SST	
			n	%	*n*	%	*n*	%
J24FS	FS	8	1	12.5	1	12.5	0	0
J28FS	FS	23	8	34.8	2	8.7	0	0
J28FR	FR	8	6	75.0	0	0	0	0
J29FR	FR	2	1	50.0	0	0	0	0
J28WGA	WGA	56	34	60.7	2	1.8	0	0
J29WGA	WGA	136	54	39.7	2	1.5	6	4.4

FR, fluororuby; FS, fluorescein; PKCδ, protein kinase C delta; SST, somatostatin; WGA, wheat germ agglutinin.

amygdala (35,39,68). For example, *Prkcd* neurons project to the CeM, and both *Prkcd* and *Sst* neurons project to the BSTLd) (Figure 4D) (32,35,39,68), suggesting that these neurons may coordinate CeL and BSTLd in mediating threat-related behaviors. Because of the lack of data in primates and the known species differences in extended amygdala organization (25), we characterized whether CeL PKCδ and SST neurons project to the BSTLd in monkeys. In 6 cases, retrograde tracers were injected into different BST subregions, and in 2 of these cases the injections were centered in the BSTLd (J29WGA and J28WGA) (Figure 4A, B). Tissue was colabeled for the retrograde tracer, DAPI, PKCδ, and SST. Consistent with our previous observations from these monkeys (25), the cases with injections directly into the BSTLd (Figure 4A, B) demonstrated substantially more CeL retrograde–labeled cells (Table 2). In these 2 cases, CeL retrograde–labeled cells expressing PKCδ ranged from 40% to 60% (Figure 4C). In contrast, few retrograde-labeled cells exclusively expressed SST or coexpressed SST and PKCδ (Figure 4C). Adding to our previous observation, SST varicosities also surrounded some CeL to BSTLd-projecting neurons, a subset of which expressed PKCδ (Figure 4D). These data demonstrate that a subset of PKCδ neurons project to the BSTLd, and that SST input likely modulates this projection.

DISCUSSION

Preclinical and clinical research has characterized the neural circuitry underlying fear and anxiety processing. In rodents, molecular studies have been performed to identify potential molecules that modulate the function of these critical neural circuits. Monkey studies are critical for translating these findings to humans, and in this regard the AT model has been extremely helpful. An essential step for understanding mechanisms associated with maladaptive anxiety and in guiding new treatment development is to systematically characterize gene expression alterations in monkeys.

Here, we used a dimensional approach in AT-phenotyped monkeys that follows the presentation of human anxiety. Our previous neuroimaging work supports the dimensionality of the AT construct at a circuit level, and our search for AT-related transcripts is based on this premise. While the subsample used here did not display the highest degree of AT, the range of AT values within the subsample is representative of the larger population. In these 47 animals, we performed RNA-Seq on neurons captured from the CeL, a region critically involved in gating threat responses (20). Consistent with our previous work (45), we find that AT predicts CeL gene expression better than each of its components alone, but also that individual genes can be component-specific or component-general. This suggests that the variance in CeL gene expression can be better explained by the behavioral and endocrine AT composite than by each AT component alone, but also that specific genes or gene modules may be AT related and still independently associated with specific AT components.

Our ontology analysis revealed overlaps between AT-associated genes and previously identified AT-related molecular pathways (41,58). Here, a number of transcripts reflect genes that are involved in epigenetic mechanisms (*SS18* and *DNMT3A*) (69,70), which is interesting because our earlier work suggested that AT-related Ce metabolism is predominantly affected by nonheritable factors (4). The current findings provide a molecular pathway by which epigenetic mechanisms may influence Ce function, which is particularly relevant to psychiatric disorders that are precipitated by stress (4,71).

We also identified *KIAA1009* and *SLC18A2* as AT related. *KIAA1009* codes for a protein located at the base of primary cilia (46); interestingly, primary cilia alterations are implicated in reduced adult neurogenesis (49), poor novel object learning (48), and schizophrenia (47,72). In addition, *SLC18A2,* which codes for VMAT2, is critical for monoaminergic neurotransmission and has been proposed as a possible drug target for some neuropsychiatric disorders (51–54). Taken together, these data support further investigation of these genes in amygdala function and psychopathology. Previously, we found an association between the truncated isoform of *NTRK3* and AT (58). However, the relatively low amount of RNA acquired with LCM precluded us from confidently examining the relations between AT and isoforms of *NTRK3.*

It is particularly exciting that CeL *PRKCD* mRNA expression was associated with AT given that numerous rodent studies demonstrate that CeL *Prkcd* neurons are part of a microcircuit that modulates freezing behavior (22,32,38,56,73). Our systematic immunohistochemical characterization revealed that 59% of primate CeL neurons express PKCδ. This raises the possibility that the relation between *PRKCD* mRNA and AT

could be accounted for by differences in the number of PKCδ neurons rather than differences in the expression level of PKCδ within the same number of PKCδ neurons. Unfortunately, because the tissue was fresh frozen for RNA-Seq, immunohistochemical staining could not be performed in the tissue from these animals.

Cross-species studies demonstrate that the CeL sends major projections to the BSTLd (23,25,33,35,39). We assessed the extent to which monkey CeL PKCδ neurons project to the BSTLd. Using retrograde tracers introduced into the BSTLd, we found that CeL PKCδ neurons constituted approximately half of the identified CeL to BSTLd-projecting neurons. These data demonstrate that PKCδ neurons originating in the CeL project to the BSTLd. Our previous studies demonstrated that the Ce and BST are part of the neural circuit underlying AT (4), and the current data suggest a plausible pathway by which the CeL interacts with the BSTLd to coordinate AT-relevant responses. It is important to consider that approximately half of the retrograde-labeled neurons did not express PKCδ, suggesting that other CeL neuronal populations could be involved in mediating AT (33,74,75). We note that while *Macaca mulatta* was used in the RNA-Seq experiment, *Macaca fascicularis* was used in the tract-tracing experiments; although the species are highly similar, this is a potential limitation.

Rodent studies point to the importance of CeL PKCδ cells in threat responding but do not address the role of the actual PKCδ protein. While the function of the PKCδ protein in threat processing is unknown, PKCδ is involved in the phospholipase C/PIP_2/diacyl glycerol pathway, a secondary messenger system shared by neurotrophic (76), chemokine, and membrane steroid signaling (77–79). Future studies manipulating CeL PKCδ expression will help discern the potential therapeutic value of targeting PKCδ.

CeL *Prkcd* neurons interact with other neuronal populations, including *Sst* neurons (22,32,38). While *SST* mRNA was not associated with AT, because of its potential modulatory role, we also systematically characterized CeL SST neurons. In the monkey, SST neurons constituted a smaller population than in the mouse; however, both species demonstrated dense CeL SST neuropil (54,64,67). We further examined monkey CeL SST varicosities and found that they have close appositions to the somata and primary dendrites of some CeL to BSTLd-projecting neurons, including PKCδ neurons. The origin of the SST innervation in the monkey CeL is unknown. However, SST is expressed in GABAergic neuronal subtypes, and a limited number of GABAergic regions send input to the CeL, including the BST, the sublenticular extended amygdala, and the amygdala intercalated cell masses (23,25,35,80,81). In addition, local CeL SST neurons may also be the source of the dense SST neuropil (22,38,66,82). Future studies that focus on understanding the origins of CeL SST input and the effects of SST release on CeL PKCδ neurons will further our understanding of primate AT-relevant microcircuits.

This transcriptome-wide study in monkey CeL neurons provides a molecular basis for understanding alterations related to the early-life risk of developing psychopathology. This is the first study to characterize gene expression in monkey CeL neurons and to implicate CeL PKCδ neurons as components of a microcircuit relevant to primate anxiety and AT. To provide a deeper understanding of primate CeL, we systematically characterized PKCδ neurons and found potentially relevant species differences. We demonstrate that a subset of CeL PKCδ neurons project to the BSTLd and may be modulated by SST. These findings present evidence supporting a primate extended amygdala microcircuit relevant to understanding human anxiety and point to specific molecules within this circuit that could serve as potential treatment targets for anxiety disorders.

ACKNOWLEDGMENTS AND DISCLOSURES

This work was supported by funding from the National Institute of Mental Health (Grant Nos. R01MH081884 and R01MH046729 [to NHK], No. R01MH063291 [to JLF], and No. 5T32MH018931 [to RK]) and by grants to the Wisconsin National Primate Center Research Center (Grant Nos. P51-OD011106 and P51-RR000167) and the California National Primate Research Center (Grant No. P51OD011107). Confocal microscopy was performed at the University of Wisconsin–Madison Biochemistry Optical Core, which was established with support from the University of Wisconsin–Madison Department of Biochemistry Endowment.

RK, ASF, JAO, PHR, and NHK conceptualized the study. NHK and ASF oversaw the study. RK, MKR, and EMF collected behavioral data. RK and DAF developed the rapid staining LCM microscopy method and collected the RNA data. DAF performed RNA extractions. JAK and his group performed RNA-Seq. TS aligned the RNA-Seq data. RK and TS analyzed the RNA-Seq data. RK, MKR, and PHR collected tissue, and PHR assessed cortisol. JLF, NHK, and RK conceptualized the stereology study. RK and CEG collected and analyzed the stereology data. JLF performed retrograde tracer surgeries and collected injected tissue. RK performed triple labeling of tracing experiments and microscopic analysis. RK and NHK wrote the manuscript.

We thank the Neuroscience Training Program at the University of Wisconsin–Madison, the personnel of the Harlow Center for Biological Psychology, the HealthEmotions Research Institute, the Waisman Laboratory for Brain Imaging and Behavior, the Wisconsin National Primate Research Center, the Wisconsin Institutes for Medical Research, S. Shelton, and H. Van Valkenberg. We thank L. Kordyban, A. Meier, J. Schnabel, and A. Elhers for help with LCM, M. Kenwood for assistance with collating and analyzing the population behavioral data, and K. Peelman for help with the mouse perfusions.

This article was published as a preprint on bioRxiv: https://doi.org/10.1101/808279.

NHK has received honoraria from CME Outfitters, Elsevier, and the Pritzker Consortium; has served on scientific advisory boards for Actify Neurotherapies and Neuronetics; currently serves as an advisor to the Pritzker Neuroscience Consortium and as a consultant to Corcept Therapeutics; has served as coeditor of Psychoneuroendocrinology and currently serves as editor-in-chief of the *American Journal of Psychiatry*; and has patents on promoter sequences for corticotropin-releasing factor CRF2α and a method of identifying agents that alter the activity of the promoter sequences (Patent Nos. 7,071,323 and 7,531,356), promoter sequences for urocortin II and the use thereof (Patent No. 7,087,385), and promoter sequences for corticotropin-releasing factor binding protein and the use thereof (Patent No. 7,122,650). The other authors report no biomedical financial interests or potential conflicts of interest.

ARTICLE INFORMATION

From the Department of Psychiatry (RK, DAF, CEG, PHR, JAO, MKR, EMF, NHK), Neuroscience Training Program (RK, PHR, NHK), and HealthEmotions Research Institute (RK, DAF, PHR, JAO, MKR, EMF, NHK), University of Wisconsin–Madison, Madison, Wisconsin; Department of Cell Biology (TS, JAK), State University of New York Downstate Medical Center, Brooklyn, New York; Department of Psychiatry (JLF) and Department of Neuroscience/Del Monte Institute for Brain Research (JLF), University of Rochester Medical Center, Rochester, New York; and Department of Psychology (ASF) and California National Primate Research Center (ASF), University of California, Davis, Davis, California.

Address correspondence to Rothem Kovner, Ph.D., Department of Psychiatry, University of Wisconsin–Madison, 6001 Research Park Blvd., Madison, WI 53719 or Ned H. Kalin, M.D., Department of Psychiatry, University of Wisconsin-Madison, 6001 Research Park Blvd., Madison, WI 53719; E-mail: kovnerrothem@gmail.com or rkovner@wisc.edu or nkalin@wisc.edu.

Received Dec 9, 2019; revised Apr 22, 2020; accepted May 10, 2020.

Supplementary material cited in this article is available online at https://doi.org/10.1016/j.biopsych.2020.05.009.

REFERENCES

1. Stein MB, Jang KL, Livesley WJ (1999): Heritability of anxiety sensitivity: A twin study. Am J Psychiatry 156:246–251.
2. Sawyers C, Ollendick T, Brotman MA, Pine DS, Leibenluft E, Carney DM, *et al.* (2019): The genetic and environmental structure of fear and anxiety in juvenile twins. Am J Med Genet B Neuropsychiatr Genet 180:204–212.
3. Eley TC, Bolton D, O'Connor TG, Perrin S, Smith P, Plomin R (2003): A twin study of anxiety-related behaviours in pre-school children. J Child Psychol Psychiatry 44:945–960.
4. Fox AS, Oler JA, Shackman AJ, Shelton SE, Raveendran M, McKay DR, *et al.* (2015): Intergenerational neural mediators of early-life anxious temperament. Proc Natl Acad Sci U S A 112:9118–9122.
5. Fox AS, Shelton SE, Oakes TR, Davidson RJ, Kalin NH (2008): Trait-like brain activity during adolescence predicts anxious temperament in primates. PLoS One 3:e2570.
6. Biederman J, Hirshfeld-Becker DR, Rosenbaum JF, Herot C, Friedman D, Snidman N, *et al.* (2001): Further evidence of association between behavioral inhibition and social anxiety in children. Am J Psychiatry 158:1673–1679.
7. Davidson RJ, Rickman M (1999): Behavioral inhibition and the emotional circuitry of the brain: Stability and plasticity during the early childhood years. In: Schmidt LA, Schulkin J, editors. Extreme Fear, Shyness, and Social Phobia: Origins, Biological Mechanisms, and Clinical Outcomes. New York: Oxford University Press, 67–87.
8. Hirshfeld DR, Rosenbaum JF, Biederman J, Bolduc EA, Faraone SV, Snidman N, *et al.* (1992): Stable behavioral inhibition and its association with anxiety disorder. J Am Acad Child Adolesc Psychiatry 31:103–111.
9. Kagan J, Reznick JS, Snidman N (1987): The physiology and psychology of behavioral inhibition in children. Child Dev 58:1459–1473.
10. Essex MJ, Klein MH, Slattery MJ, Goldsmith HH, Kalin NH (2010): Early risk factors and developmental pathways to chronic high inhibition and social anxiety disorder in adolescence. Am J Psychiatry 167:40–46.
11. Chronis-Tuscano A, Degnan KA, Pine DS, Perez-Edgar K, Henderson HA, Diaz Y, *et al.* (2009): Stable early maternal report of behavioral inhibition predicts lifetime social anxiety disorder in adolescence. J Am Acad Child Adolesc Psychiatry 48:928–935.
12. Fox NA, Henderson HA, Marshall PJ, Nichols KE, Ghera MM (2005): Behavioral inhibition: Linking biology and behavior within a developmental framework. Annu Rev Psychol 56:235–262.
13. Fox AS, Kalin NH (2014): A translational neuroscience approach to understanding the development of social anxiety disorder and its pathophysiology. Am J Psychiatry 171:1162–1173.
14. Kalin NH, Shelton SE (2003): Nonhuman primate models to study anxiety, emotion regulation, and psychopathology. Ann N Y Acad Sci 1008:189–200.
15. Oler JA, Fox AS, Shelton SE, Rogers J, Dyer TD, Davidson RJ, *et al.* (2010): Amygdalar and hippocampal substrates of anxious temperament differ in their heritability. Nature 466:864–868.
16. Hettema JM, Neale MC, Kendler KS (2001): A review and meta-analysis of the genetic epidemiology of anxiety disorders. Am J Psychiatry 158:1568–1578.
17. Janak PH, Tye KM (2015): From circuits to behaviour in the amygdala. Nature 517:284–292.
18. Fox AS, Oler JA, Tromp DPM, Fudge JL, Kalin NH (2015): Extending the amygdala in theories of threat processing. Trends Neurosci 38:319–329.
19. Alheid GF, Heimer L (1988): New perspectives in basal forebrain organization of special relevance for neuropsychiatric disorders: The striatopallidal, amygdaloid, and corticopetal components of substantia innominata. Neuroscience 27:1–39.
20. Fadok JP, Markovic M, Tovote P, Luthi A (2018): New perspectives on central amygdala function. Curr Opin Neurobiol 49:141–147.
21. Viviani D, Charlet A, van den Burg E, Robinet C, Hurni N, Abatis M, *et al.* (2011): Oxytocin selectively gates fear responses through distinct outputs from the central amygdala. Science 333:104–107.
22. Fadok JP, Krabbe S, Markovic M, Courtin J, Xu C, Massi L, *et al.* (2017): A competitive inhibitory circuit for selection of active and passive fear responses. Nature 542:96–100.
23. Petrovich GD, Swanson LW (1997): Projections from the lateral part of the central amygdalar nucleus to the postulated fear conditioning circuit. Brain Res 763:247–254.
24. Veening JG, Swanson LW, Sawchenko PE (1984): The organization of projections from the central nucleus of the amygdala to brainstem sites involved in central autonomic regulation: A combined retrograde transport-immunohistochemical study. Brain Res 303:337–357.
25. Oler JA, Tromp DP, Fox AS, Kovner R, Davidson RJ, Alexander AL, *et al.* (2017): Connectivity between the central nucleus of the amygdala and the bed nucleus of the stria terminalis in the non-human primate: Neuronal tract tracing and developmental neuroimaging studies. Brain Struct Funct 222:21–39.
26. Dong HW, Petrovich GD, Swanson LW (2001): Topography of projections from amygdala to bed nuclei of the stria terminalis. Brain Res Brain Res Rev 38:192–246.
27. Kim SY, Adhikari A, Lee SY, Marshel JH, Kim CK, Mallory CS, *et al.* (2013): Diverging neural pathways assemble a behavioural state from separable features in anxiety. Nature 496:219–223.
28. Kalin NH, Shelton SE, Davidson RJ (2004): The role of the central nucleus of the amygdala in mediating fear and anxiety in the primate. J Neurosci 24:5506–5515.
29. Kalin NH, Shelton SE, Davidson RJ, Kelley AE (2001): The primate amygdala mediates acute fear but not the behavioral and physiological components of anxious temperament. J Neurosci 21:2067–2074.
30. Amaral DG, Price JL, Pitkanen A, Carmichael ST (1993): Anatomical organization of the primate amygdaloid complex. In: Aggleton JP, editor. The Amygdala: Neurobiological Aspects of Emotion, Memory, and Mental Dysfunction. New York: Wiley–Liss, 1–66.
31. De Olmos JS (2004): The amygdala. In: Paxinos G, Mai JK, editors. The Human Nervous System, 2nd ed. San Diego: Elsevier Academic Press, 739–860.
32. Haubensak W, Kunwar PS, Cai H, Ciocchi S, Wall NR, Ponnusamy R, *et al.* (2010): Genetic dissection of an amygdala microcircuit that gates conditioned fear. Nature 468:270–276.
33. Pomrenze MB, Tovar-Diaz J, Blasio A, Maiya R, Giovanetti SM, Lei K, *et al.* (2019): A corticotropin releasing factor network in the extended amygdala for anxiety. J Neurosci 39:1030–1043.
34. Asok A, Draper A, Hoffman AF, Schulkin J, Lupica CR, Rosen JB (2018): Optogenetic silencing of a corticotropin-releasing factor pathway from the central amygdala to the bed nucleus of the stria terminalis disrupts sustained fear. Mol Psychiatry 23:914–922.
35. Ahrens S, Wu MV, Furlan A, Hwang GR, Paik R, Li H, *et al.* (2018): A central extended amygdala circuit that modulates anxiety. J Neurosci 38:5567–5583.
36. Yu K, Ahrens S, Zhang X, Schiff H, Ramakrishnan C, Fenno L, *et al.* (2017): The central amygdala controls learning in the lateral amygdala. Nat Neurosci 20:1680–1685.
37. LeDoux JE, Cicchetti P, Xagoraris A, Romanski LM (1990): The lateral amygdaloid nucleus: Sensory interface of the amygdala in fear conditioning. J Neurosci 10:1062–1069.
38. Li H, Penzo MA, Taniguchi H, Kopec CD, Huang ZJ, Li B (2013): Experience-dependent modification of a central amygdala fear circuit. Nat Neurosci 16:332–339.
39. Ye J, Veinante P (2019): Cell-type specific parallel circuits in the bed nucleus of the stria terminalis and the central nucleus of the amygdala of the mouse. Brain Struct Funct 224:1067–1095.

40. Funk CM, Peelman K, Bellesi M, Marshall W, Cirelli C, Tononi G (2017): Role of somatostatin-positive cortical interneurons in the generation of sleep slow waves. J Neurosci 37:9132–9148.
41. Fox AS, Oler JA, Shelton SE, Nanda SA, Davidson RJ, Roseboom PH, *et al.* (2012): Central amygdala nucleus (Ce) gene expression linked to increased trait-like Ce metabolism and anxious temperament in young primates. Proc Natl Acad Sci U S A 109:18108–18113.
42. Zimin AV, Cornish AS, Maudhoo MD, Gibbs RM, Zhang X, Pandey S, *et al.* (2014): A new rhesus macaque assembly and annotation for next-generation sequencing analyses. Biol Direct 9:20.
43. Love MI, Huber W, Anders S (2014): Moderated estimation of fold change and dispersion for RNA-seq data with DESeq2. Genome Biol 15:550.
44. Mi H, Muruganujan A, Ebert D, Huang X, Thomas PD (2018): PANTHER version 14: More genomes, a new PANTHER GO-slim and improvements in enrichment analysis tools. Nucleic Acids Res 47:D419–D426.
45. Shackman AJ, Fox AS, Oler JA, Shelton SE, Davidson RJ, Kalin NH (2013): Neural mechanisms underlying heterogeneity in the presentation of anxious temperament. Proc Natl Acad Sci U S A 110:6145–6150.
46. Wang WJ, Tay HG, Soni R, Perumal GS, Goll MG, Macaluso FP, *et al.* (2013): CEP162 is an axoneme-recognition protein promoting ciliary transition zone assembly at the cilia base. Nat Cell Biol 15:591–601.
47. Munoz-Estrada J, Lora-Castellanos A, Meza I, Alarcon Elizalde S, Benitez-King G (2018): Primary cilia formation is diminished in schizophrenia and bipolar disorder: A possible marker for these psychiatric diseases. Schizophr Res 195:412–420.
48. Wang Z, Phan T, Storm DR (2011): The type 3 adenylyl cyclase is required for novel object learning and extinction of contextual memory: Role of cAMP signaling in primary cilia. J Neurosci 31:5557–5561.
49. Amador-Arjona A, Elliott J, Miller A, Ginbey A, Pazour GJ, Enikolopov G, *et al.* (2011): Primary cilia regulate proliferation of amplifying progenitors in adult hippocampus: Implications for learning and memory. J Neurosci 31:9933–9944.
50. Berbari NF, Malarkey EB, Yazdi SM, McNair AD, Kippe JM, Croyle MJ, *et al.* (2014): Hippocampal and cortical primary cilia are required for aversive memory in mice. PLoS One 9:e106576.
51. Duman RS, Li N (2012): A neurotrophic hypothesis of depression: Role of synaptogenesis in the actions of NMDA receptor antagonists. Philos Trans R Soc Lond B Biol Sci 367:2475–2484.
52. Newton AC (2010): Protein kinase C: Poised to signal. Am J Physiol Endocrinol Metab 298:E395–E402.
53. Amano T, Amir A, Goswami S, Pare D (2012): Morphology, PKCδ expression, and synaptic responsiveness of different types of rat central lateral amygdala neurons. J Neurophysiol 108:3196–3205.
54. Cassel MD, Gray TS (1989): Morphology of peptide immunoreactive neurons in the rat central nucleus of the amygdala. J Comp Neurol 281:320–333.
55. Cui Y, Lv G, Jin S, Peng J, Yuan J, He X, *et al.* (2017): A central amygdala-substantia innominata neural circuitry encodes aversive reinforcement signals. Cell Rep 21:1770–1782.
56. Yu K, Garcia da Silva P, Albeanu DF, Li B (2016): Central amygdala somatostatin neurons gate passive and active defensive behaviors. J Neurosci 36:6488–6496.
57. Turner CA, Clinton SM, Thompson RC, Watson SJ Jr, Akil H (2011): Fibroblast growth factor-2 (FGF2) augmentation early in life alters hippocampal development and rescues the anxiety phenotype in vulnerable animals. Proc Natl Acad Sci U S A 108:8021–8025.
58. Fox AS, Souaiaia T, Oler JA, Kovner R, Kim JMH, Nguyen J, *et al.* (2019): Dorsal Amygdala Neurotrophin-3 Decreases Anxious Temperament in Primates. Biol Psychiatry 86:881–889.
59. Price JL, Russchen FT, Amaral DG (1987): The limbic region: II. The amygdaloid complex. In: Hokfelt BT, Swanson LW, editors. Handbook of Chemical Neuroanatomy. Amsterdam: Elsevier, 279–381.
60. Roberts GW, Woodhams PL, Polak JM, Crow TJ (1982): Distribution of neuropeptides in the limbic system of the rat: The amygdaloid complex. Neuroscience 7:99–131.
61. McCullough KM, Morrison FG, Hartmann J, Carlezon WA Jr, Ressler KJ (2018): Quantified coexpression analysis of central amygdala subpopulations. eNeuro 5:ENEURO.0010-18.2018.
62. Kim J, Zhang X, Muralidhar S, LeBlanc SA, Tonegawa S (2017): Basolateral to central amygdala neural circuits for appetitive behaviors. Neuron 93:1464–1479.e5.
63. Han W, Tellez LA, Rangel MJ Jr, Motta SC, Zhang X, Perez IO, *et al.* (2017): Integrated control of predatory hunting by the central nucleus of the amygdala. Cell 168:311–324.e18.
64. Amaral DG, Avendano C, Benoit R (1989): Distribution of somatostatin-like immunoreactivity in the monkey amygdala. J Comp Neurol 284:294–313.
65. Kovner R, Fox AS, French DA, Roseboom PH, Oler JA, Fudge JL, *et al.* (2019): Somatostatin gene and protein expression in the non-human primate central extended amygdala. Neuroscience 400:157–168.
66. Cassell MD, Gray TS, Kiss JZ (1986): Neuronal architecture in the rat central nucleus of the amygdala: A cytological, hodological, and immunocytochemical study. J Comp Neurol 246:478–499.
67. Martin LJ, Powers RE, Dellovade TL, Price DL (1991): The bed nucleus-amygdala continuum in human and monkey. J Comp Neurol 309:445–485.
68. Cai H, Haubensak W, Anthony TE, Anderson DJ (2014): Central amygdala PKC-δ(+) neurons mediate the influence of multiple anorexigenic signals. Nat Neurosci 17:1240–1248.
69. Lubieniecka JM, de Bruijn DRH, Su L, van Dijk AHA, Subramanian S, van de Rijn M, *et al.* (2008): Histone deacetylase inhibitors reverse SS18-SSX–mediated polycomb silencing of the tumor suppressor—early growth response 1—in synovial sarcoma. Cancer Res 68:4303–4310.
70. Tang L, Nogales E, Ciferri C (2010): Structure and function of SWI/SNF chromatin remodeling complexes and mechanistic implications for transcription. Prog Biophys Mol Biol 102:122–128.
71. Elbau IG, Cruceanu C, Binder EB (2019): Genetics of resilience: Gene-by-environment interaction studies as a tool to dissect mechanisms of resilience. Biol Psychiatry 86:433–442.
72. Pruski M, Lang B (2019): Primary cilia—An underexplored topic in major mental illness. Front Psychiatry 10:104.
73. Ciocchi S, Herry C, Grenier F, Wolff SB, Letzkus JJ, Vlachos I, *et al.* (2010): Encoding of conditioned fear in central amygdala inhibitory circuits. Nature 468:277–282.
74. Gray TS, Magnuson DJ (1992): Peptide immunoreactive neurons in the amygdala and the bed nucleus of the stria terminalis project to the midbrain central gray in the rat. Peptides 13:451–460.
75. Moga MM, Gray TS (1985): Evidence for corticotropin-releasing factor, neurotensin, and somatostatin in the neural pathway from the central nucleus of the amygdala to the parabrachial nucleus. J Comp Neurol 241:275–284.
76. Rankin SL, Guy CS, Rahimtula M, Mearow KM (2008): Neurotrophin-induced upregulation of p75NTR via a protein kinase C-delta-dependent mechanism. Brain Res 1217:10–24.
77. Kanehisa M, Goto S (2000): KEGG: Kyoto Encyclopedia of Genes and Genomes. Nucleic Acids Res 28:27–30.
78. Kanehisa M, Sato Y (2020): KEGG Mapper for inferring cellular functions from protein sequences. Protein Sci 29:28–35.
79. Greene MW, Morrice N, Garofalo RS, Roth RA (2004): Modulation of human insulin receptor substrate-1 tyrosine phosphorylation by protein kinase Cdelta. Biochem J 378:105–116.
80. Pare D, Smith Y (1993): The intercalated cell masses project to the central and medial nuclei of the amygdala in cats. Neuroscience 57:1077–1090.
81. Gungor NZ, Yamamoto R, Pare D (2015): Optogenetic study of the projections from the bed nucleus of the stria terminalis to the central amygdala. J Neurophysiol 114:2903–2911.
82. Gray TS, Cassell MD, Williams TH (1982): Synaptology of three peptidergic neuron types in the central nucleus of the rat amygdala. Peptides 3:273–281.
83. Paxinos G, Huang X, Petrides M, Toga AW (2009): The Rhesus Monkey Brain: Stereotaxic Coordinates. San Diego: Elsevier.
84. Schindelin J, Arganda-Carreras I, Frise E, Kaynig V, Longair M, Pietzsch T, *et al.* (2012): Fiji: An open-source platform for biological-image analysis. Nat Methods 9:676–682.